ACS OMEGA

http://pubs.acs.org/journal/acsodf

Article

# Cu(I) Metal–Organic Framework Composites with AgCl/Ag Nanoparticles for Irradiation-Enhanced Antibacterial Activity against *E. coli*

Fangxin Mao, Yonghua Su, Xiaoying Sun, Bin Li,* and Peng Fei Liu*

Cite This: *ACS Omega* 2023, 8, 2733–2739

Read Online

ACCESS | Metrics & More | Article Recommendations | Supporting Information

**ABSTRACT:** Metal–organic frameworks (MOFs) have emerged as prospective antibacterial agents or synergistic agents for their versatile chemical building components and structures. In this work, copper(I) halide MOFs of Cu(I)bpyCl (bpy = 4,4′-bipyridine) composited with AgCl/Ag nanoparticles were synthesized, and their antibacterial activities were measured against *Escherichia coli* and *Staphylococcus aureus*. The attached chlorine in $Cu(I)_2Cl_2$ nodes of the MOFs served as loading sites for silver ions, in which AgCl and concomitant metallic Ag nanoparticles were in situ generated. Exceptional antibacterial activity against *E. coli* was realized with a minimum inhibitory concentration (MIC) of ∼7.8 $\mu g\ mL^{-1}$, while the MIC value was ∼16 $\mu g\ mL^{-1}$ against *S. aureus*. Enhanced antibacterial activity against *E. coli* with light irradiation was measured by the disk diffusion method compared with that under dark conditions.

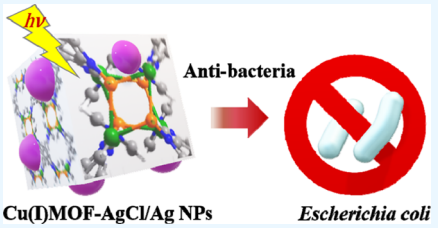


## INTRODUCTION

Antibacterial materials have been developed appreciably to protect human beings from infections caused by bacteria, especially *Escherichia coli* (Gram-negative) and *Staphylococcus aureus* (Gram-positive), common bacteria associated with public health, food, and the environment.[1,2] Using antibiotics is currently the main measure to resist bacteria, which could cause side effects and even lead to superbugs. Therefore, novel antibacterial materials that circumvent these disadvantages are required.[3] In this case, inorganic nanoparticles have attracted the attention of researchers and present prospects for defense against bacteria.[4] Silver, one of the antibacterial agents, has been used for burn treatment over the centuries.[5] Besides applications in food packaging, refrigerators, washing machines, etc., silver components are commonly used to prevent contamination. With the development of nanotechnology, nanoscale silver materials were proven to possess enhanced activity and are valuable for use in medical and healthcare areas.[6,7] Considering the possible cytotoxic effects on human and environmental health, many functionalizations such as particle size and coating engineering were carried out to reduce their negative effect, which also increased their antibacterial capacity and selectivity.[7] It is very significant to develop highly active silver antibacterial agents with a low dose necessary for immunologic defense.

The exact antibacterial mechanism of silver-based agents is still not known, although there is evidence of different mechanisms because of their physicochemical properties. The release of silver ions from silver-based complexes is considered a critical matter in the antibacterial mechanism, in which metallic silver could be oxidized to the cation under environmental conditions.[8−10] Silver ions can interact with cellular components to inhibit or kill bacteria by altering the cell membrane, protein activity, metabolic pathways, and even genetic material. To kill bacteria, passive release and stimuli-responsive release strategies were developed based on the structure of silver composites and the local microenvironment (e.g., pH, enzymes, glutathione, etc.) of bacterial infection. One of the stimuli-responsive solutions involves exogenous triggers using external factors such as light irradiation to control silver ion release and thus improve the antibacterial effect.[10] As plasmonic particles, the silver surface plasmon resonance (SPR) effect[11,12] endows them with excellent photocatalytic activity, which could be enhanced by a heterogeneous halide structure.[13] Ag/AgX (X = Cl, Br and I) nanostructures were reported to have the ability to absorb visible light over a broad range and produce reactive oxygen species and reactive chlorine species to kill bacteria.[14] Other semiconductors such as ZnO,[15,16] $TiO_2$,[17] BiOCl,[18] $W_{18}O_{49}$,[19] etc., could achieve effective antibacterial performance via a synergistic mechanism for silver-based agents. Low-dimensional structures, such as two-dimensional nanomaterials, have been widely studied as photocatalytic antibacterial agents by regulating their structure and components.[20] Constructing a

Received: November 18, 2022
Accepted: December 22, 2022
Published: January 4, 2023





https://doi.org/10.1021/acsomega.2c07415
*ACS Omega* 2023, 8, 2733−2739

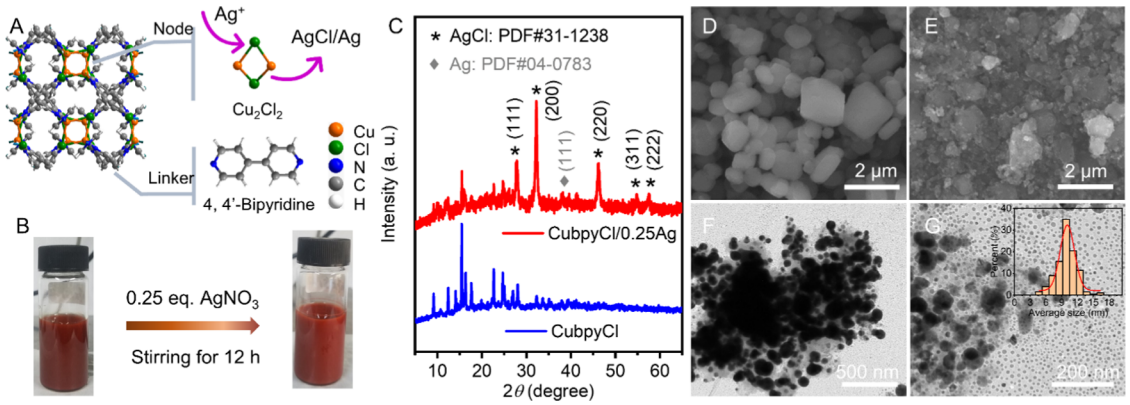


**Figure 1.** (A) Schematic diagram of the CubpyCl/Ag composite showing the $Ag^+$ ions attacking the halide nodes of Cu(I)-MOF. (B) Digital image of the CubpyCl/0.25Ag sample prepared from CubpyCl. (C) XRD patterns of CubpyCl and CubpyCl/0.25Ag, in which remarkable AgCl and slight Ag characterization peaks exist. (D, E) Scanning electron microscopy (SEM) images of CubpyCl and CubpyCl/0.25Ag. (F, G) Transmission electron microscopy (TEM) images of CubpyCl/0.25Ag. The inset prevents an average of 10 nm for the smaller nanoparticles in (G).

light-responsive matrix with silver nanomaterials presents a promising pathway for high-efficiency antibacterial agents.

Recently, metal−organic frameworks (MOFs) have emerged as third-generation antibacterial agents beyond inorganic materials because of their porous properties and various metallic and ligand components endowing them with abundant functions.[21] Zn/Al-terephthalate MOF,[22,23] Cu/benzene-1,3,5-tricarboxylic acid MOF,[24] and Cu and CuZn-terephthalic acid-1,4-diazabicyclo[2.2.2]octane multi-metal and ligand MOF[25] have been reported to possess antimicrobial activity. MOFs can also provide a good reservoir and synergic platform for antibacterial agents due to their photic and chemical features.[26] Photoresponsive MOF material platforms have demonstrated efficient bacterial capture and photothermal killing effects.[27,28] Organic link modification,[29] pore-filling,[30] and surface-coating[31] strategies were reported to improve the antibacterial activity. Attaching Ag species to MOFs is expected to be a promising strategy for developing antibacterial materials.

Cu-based MOFs containing divalent metal ions were reported to function as antibacterial materials, with bactericidal ability and biocompatibility of the metal component.[32,33] However, monovalent copper $Cu^+$ has scarcely been used in MOFs, although its better antibacterial effect compared with divalent Cu ions has been verified.[34,35] Further, copper(I) complexes generally display luminescent behavior due to their $d^{10}$ electronic configuration, and copper(I) halide aggregates have also been reported to serve as photosensitizers and cocatalysts.[36,37] This light-responsive property could provide an exogenous trigger to enhance the sterilization effect. Therefore, Cu(I)MOF incorporated with Ag species could be prospective candidates with efficient antibacterial performances. Herein, we prepare Cu(I)MOF-AgCl/Ag materials by in situ anchoring Ag ions into chloro-bridged Cu(I) nodes of MOFs, thereby generating AgCl/Ag nanoparticles in the frameworks. The minimum inhibitory concentration (MIC) and disk diffusion method measurements revealed the expected antibacterial activity against *E. coli* and *S. aureus*, and a selectively enhanced performance was observed against *E. coli* with light irradiation.

## EXPERIMENTAL SECTION

**Material and Methods.** *Synthesis of CubpyCl (bpy = 4,4′-Bipyridine) MOF.* The copper(I) halide aggregate of CubpyCl (bpy = 4,4′-bipyridine) was prepared through a solution diffusion method according to an earlier report.[38] Typically, 5.0 mmol (0.50 g) of CuCl was added into 50 mL of acetonitrile under magnetic stirring in a 100 mL screwed-lid jar. A Pistac turbid solution could be observed after 10 min of stirring due to the limited solubility of CuCl in acetonitrile; 5.0 mmol (0.78 g) of bpy ligand was dissolved in 10 mL of acetonitrile, leading to a clear solution. The bpy solution was poured into the screwed-lid jar, and a dark-red product formed immediately. After stirring for another 30 min, the solids were separated and washed with ethyl ether twice by centrifugation (7000 rpm, 10 min) and then dried under vacuum at 60 °C.

*Synthesis of CubpyCl Composited with AgCl/Ag Nanoparticles.* The atomic ratios of Ag to Cu were roughly controlled at 0.25, 1.0, and 2.0 by their precursor feed quantity. In detail, 10/40/80 mg of $AgNO_3$ was dissolved in 15 mL of ethyl alcohol, and 50 mg of the prepared CubpyCl powder was dispersed into the solution by simple ultrasonic dispersion in a 30 mL screwed-lid jar. Under continuous magnetic stirring, the colors of the three samples gradually changed with time. Especially, the samples with 40 and 80 mg of $AgNO_3$ become green in color after 12 h. The solids were collected by centrifugation with ethyl alcohol two times and dried in a vacuum oven at 60 °C.

**Antibacterial Activity Assay.** *Minimum Inhibitory Concentration (MIC) Measurements.* The MICs against *E. coli* and *S. aureus* were determined by a broth dilution method. MIC refers to the lowest concentration of the agent where no visible bacterial growth is observed after incubation at 37 °C. Typically, a 96-well plate was used and 100 μL of Luria Bertani (LB) broth was added to all holes except the first one. The sample solution is mixed in the first hole; then, 100 μL from the first hole is transferred to the second hole, and so on, until the 10th hole, from which 100 μL is drawn out. Bacteria are added and diluted 500 times (0.2%). Finally, 100 μL of the bacterial solution was added to the 96-well plate. Then, 100 μL of aseptic distilled water was added into the 11th hole as the negative control, and 100 μL of bacterial solution was inoculated into the 12th hole as the bacterial growth control. The bacteria were cultured for 12−16 h after 10 min illumination under 37 °C. Bacterial growth was confirmed if there was turbidity or precipitation compared with the negative control. Aseptic growth would be confirmed if its transparency was the same as the negative control.


https://doi.org/10.1021/acsomega.2c07415
ACS Omega 2023, 8, 2733−2739

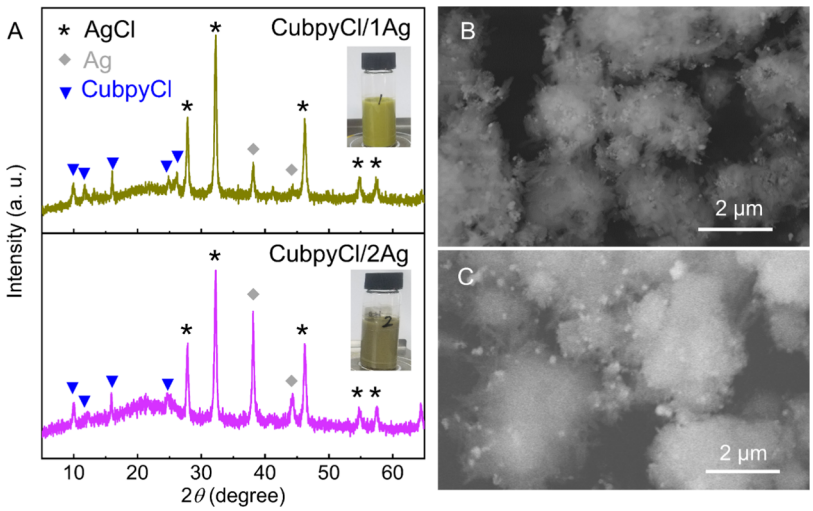


**Figure 2.** (A) XRD patterns of the prepared CubpyCl/1Ag and CubpyCl/2Ag. The samples turn into an olive color with increased load of $Ag^+$ ions, and the peaks of Ag become more intense. (B, C) SEM images of CubpyCl/1Ag and CubpyCl/2Ag.

*Disk Diffusion Method.* The antibacterial activity of the samples was investigated by the disk diffusion technique under dark and light conditions. A sterile cotton swab was used to inoculate bacteria onto the surface of LB broth plates. The as-compared compounds (4 mg) were suspended in sterile water and placed over the surface of the plates to maintain contact with bacteria. For the light-irradiated group, the plate was irradiated under a 300 W Xe lamp for 5 min before incubation. The diameter of the inhibition zone was measured after 24 h of incubation at 37 °C, which enabled the evaluation of the antibacterial activity.

## RESULTS AND DISCUSSION

AgCl was incorporated into the MOF frameworks by the anchoring sites of halogen in the MOF nodes. Copper(I) chloride and the bridging ligand of 4,4′-bipyridine (bpy) assemble into a three-dimensional network, wherein chloro-bridged Cu(I) dimers provide loading sites to Ag ions.[38,39] A schematic diagram of hybrid materials is shown in Figure 1A; $Ag^+$ ions could access the halide node through the pores of the MOF and form AgCl nanoparticles located in the cavities. Based on the Cu(I) molar equivalent of the MOF, a quarter of the $AgNO_3$ was introduced into the CubpyCl-containing ethanol solution, and the color change could be observed, as shown in Figure 1B. The elemental contents were estimated by energy-dispersive spectroscopy (EDS) analysis, as shown in Figures S1 and S2, which demonstrated the successful integration of Ag into CubpyCl. The relative atomic proportion of Ag:Cu is close to the expected ratio (Tables S1 and S2). As shown in Figure 1C, X-ray diffraction (XRD) patterns of the CubpyCl sample show the typical crystalline phase of the copper(I) halide MOF, as reported earlier,[37] and XRD patterns of CubpyCl/0.25Ag reveal that cubic AgCl can be produced in the frameworks as the MOF phase survived. The characteristic peaks at 27.8, 32.2, 46.2, 54.8, and 57.5° are consistent with standard AgCl (PDF#31-1238) facets of (111), (200), (220), (311), and (222), correspondingly. A faint peak at 38.1° may be assigned to metallic Ag (PDF#04-0783) nanoparticles due to their small size or low content, which can be verified by the results of the sample with increased Ag ratios.

The morphologies of CubpyCl and CubpyCl/0.25Ag were investigated by scanning electron microscopy (SEM) and transmission electron microscopy (TEM) measurements. CupbyCl presents sizes of 0.5−2 $\mu$m with a smooth surface (Figure 1D). The morphology of CubpyCl changes after introducing silver ions, and small-sized particles with different contrasts appear in CubpyCl/0.25Ag, as shown in the SEM image in Figure 1E. In the TEM image of CubpyCl/0.25Ag (Figure 1F), about 100 nm AgCl nanoparticles can be observed in the MOF matrix, and ultrasmall particles with an average size of 10 nm, measured from high-magnification TEM images (Figure 1G), could be affirmed as Ag particles based on the Scherrer law according to the XRD results (Figure 1C). Based on the reaction in the process, silver ions may attack the halogen in the nodes of CubpyCl MOFs, resulting in the in situ formation of AgCl nanoparticles, while local initial frameworks may collapse and be replaced by inorganic particles. As shown in Figure S4, the inorganic particles are coated by the MOF matrix and present different contrasts. Therefore, the proposed schematic diagram could be demonstrated based on these results.

The increased-Ag-containing samples with 1 and 2 molar equiv of $AgNO_3$ were prepared as shown in Figure S3; the color turned gradually from red to green along with stirring time. The energy-dispersive spectroscopy (EDS) results reveal that relative contents of Ag are prominently higher than the required quantity and copper on the surface of the material (Figures S5 and S6; Tables S3 and S4). Inductively coupled plasma optical emission spectrometry (ICP-OES) was performed to measure the relative proportion of Ag to Cu, revealing the approximate ratio with the expected reagent feeding (Table S5). XRD patterns of CubpyCl/1Ag and CubpyCl/2Ag demonstrate the reserved CubpyCl phase with the diffraction peaks at 10.0, 12.2, and 15.8° (Figure 2A). Besides AgCl, sharp peaks occur at 38.1 and 44.3°, which can be attributed to the (111) and (200) characteristic planes of cubic Ag (PDF#04-0783). The enhanced peak intensity of Ag proves its increased particle size. SEM images of CubpyCl/1Ag and CubpyCl/2Ag (Figure 2B,C) exhibit a cotton morphology with nanoparticle decoration. Compared with the CubpyCl/0.25 sample, the structures of CubpyCl/1Ag and CubpyCl/2Ag are seemingly reconstituted from CubpyCl, but by loading


https://doi.org/10.1021/acsomega.2c07415
ACS Omega 2023, 8, 2733−2739

AgCl/Ag particles into MOF. The second building units of the chloro-bridged Cu(I) dimers could be disrupted, while the replacement of Cu(I) by Ag(I) might be achieved as the characteristic XRD of CubpyCl was retained although excess Ag ions were imported. To evaluate the stability of materials, XRD spectra were recorded after soaking samples in water for 48 h. As shown in Figure S7, the retained characteristic peaks of MOF exhibit acceptable stability.

TEM images of CubpyCl/1Ag present a morphology similar to that of CubpyCl/0.25Ag, where AgCl and Ag nanoparticles can be observed (Figure 3A,B). For CubpyCl/2Ag, a larger

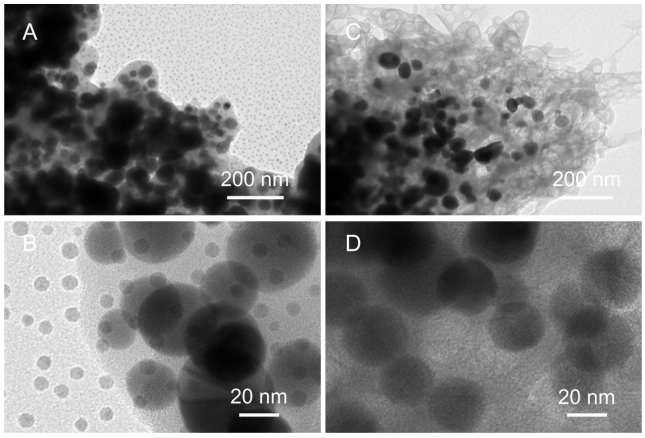


**Figure 3.** TEM images of (A, B) CubpyCl/1Ag and (C, D) CubpyCl/2Ag. Particles with a larger size could be formed due to the increased introduction of silver ions into the MOF matrix.

number of round pores are formed in the MOF, and the smallest nanoparticle size is as large as 20 nm (Figure 3C,D), which is coincident with the sharp diffraction peaks in its XRD result. Most of the AgCl/Ag nanoparticles could be coated by MOFs and were fixed in the frameworks.

The X-ray photoelectron spectroscopy (XPS) spectra of CubpyCl, CubpyCl/0.25Ag, and CubpyCl/2Ag samples were recorded, as shown in Figure S8. For the Cu 2p spectra, the intensity decreased along with an increase in the amount of silver ions introduced. The peaks shift toward higher energies after loading silver, revealing that slight oxidation of copper ions occurs in the synthetic process. In the Ag 3d spectra, Ag(0) and Ag(I) states exist in CubpyCl/0.25Ag, and in CubpyCl/2Ag samples, these peaks shift to higher energies because of a higher proportion of Ag(I). The signal attenuation of the peaks of Cu, Cl, and N elements demonstrates the reduction of their relative amounts on the surface of the material.

To evaluate the antimicrobial activity of the as-prepared materials, the MIC values were determined against *S. aureus* and *E. coli* bacteria. As shown in Figure 4A and the inset table, an MIC value of 0.5 mg $mL^{-1}$ was attained for CubpyCl against both bacteria, which indicated poor activity and so excessive dosage would be needed to keep both under control. For the samples containing silver, the MIC values decrease drastically with increasing content of silver, reducing to as low as 0.016 and 0.0078 mg $mL^{-1}$ for CubpyCl/2Ag against *S. aureus* and *E. coli*, respectively. Meanwhile, the MIC values of *E. coli* are half of that of *S. aureus* for CubpyCl/1Ag and CubpyCl/2Ag samples, which illustrates higher sensitivity against *E. coli* in comparison with *S. aureus*. Therefore, CubpyCl MOF composited with AgCl/Ag nanoparticles serves as a good and selective antimicrobial candidate material against *E. coli*.

Effect of light irradiation on the antibacterial activity was further investigated by the disk diffusion method using *S. aureus* and *E. coli*. For the prepared samples of CubpyCl/0.25Ag, CubpyCl/1Ag, and CubpyCl/2Ag, inhibition zones with different diameters occur, with an antibacterial effect like that of kanamycin, while pure CubpyCl and sterile water present nonactivity (Figure 4B). Under dark conditions, the antibacterial activity reduces along with the increased ratio of Ag/Cu in samples, that the inhibition zones diminish. Under light irradiation, the antibacterial activity is enhanced with an increased content of AgCl/Ag, and CubpyCl/2Ag shows optimal activity against *E. coli* (Figure 4C). For *S. aureus*, no obvious difference can be found with light or without light (Figure S9), which indicates no light enhancement of the antibacterial activity. The SEM images were also recorded after the antibacterial test against *E. coli* under light, as shown in Figure S10.

The morphology of *E. coli* was analyzed by SEM characterization to address the antibacterial effect of light irradiation on the materials. On light irradiation, damage to the cell membrane occurs in *E. coli*, as presented in Figure S11 (marked with yellow arrows). Light irradiation could injure cells but not kill them. On introducing CubpyCl, some *E. coli* bacteria were killed and their cell membranes were fragmented and wrinkled, as shown in Figure 5A. More dead bacteria could be observed in Figure 5E, which reveals the enhancement by light irradiation. The damage to the cell membrane might be caused by Cu ions released from the MOFs.[40,41] The CubpyCl materials show the capacity for killing *E. coli* bacteria, although a few surviving bacteria could still be found. When Ag was incorporated into CubpyCl, severe shrinking of the morphology of bacteria was observed, as shown in Figure 5B−D,F−H, which demonstrates their outstanding antibacterial effects. In the light irradiation group, more nanoparticles were present around E. coli, preventing their normal growth. These SEM results provide solid evidence for the antibacterial activity of Cu(I)MOF-AgCl/Ag materials.

To explore the underlying mechanism of the photocatalytic process, light absorption spectra were recorded, as shown in Figure S12. All samples present similar absorption bands below 300 nm. In the visible-light region, CubpyCl exhibits a typical broad absorption peak around 540 nm. The spectrum displays a blue-shifting trend along with increasing incorporation of silver species. The CubpyCl/2Ag sample shows a typical absorption peak around 447 nm, which can be assigned to the absorption of silver nanoparticles.[42,43] The semiconductive Cu(I)-Cl-bpy MOF exhibits a bandgap energy of about 1.85 eV, and $Cu(I)_2Cl_2$ clusters in the frameworks could serve as photoelectron generators.[37] Benefiting from the SPR Ag, the Cu(I)MOFs-AgCl/Ag system may establish a plasmonic Z-scheme photocatalytic process for enhancing the activity.[44−46] Light can improve the activity of Ag materials by accelerating $Ag^+$ release, thereby increasing the decomposition of AgCl.[47,48] The generated $Cl^-$ ions impede the destruction of bacteria by silver particles, while higher activity is observed under light conditions. It could be speculated that the CubpyCl matrix may synergistically improve the antibacterial activity.

## CONCLUSIONS

Herein, Cu(I)MOF-AgCl/Ag composites have been developed by anchoring AgCl/Ag onto nodes of the MOF. The chloro-


https://doi.org/10.1021/acsomega.2c07415
ACS Omega 2023, 8, 2733−2739

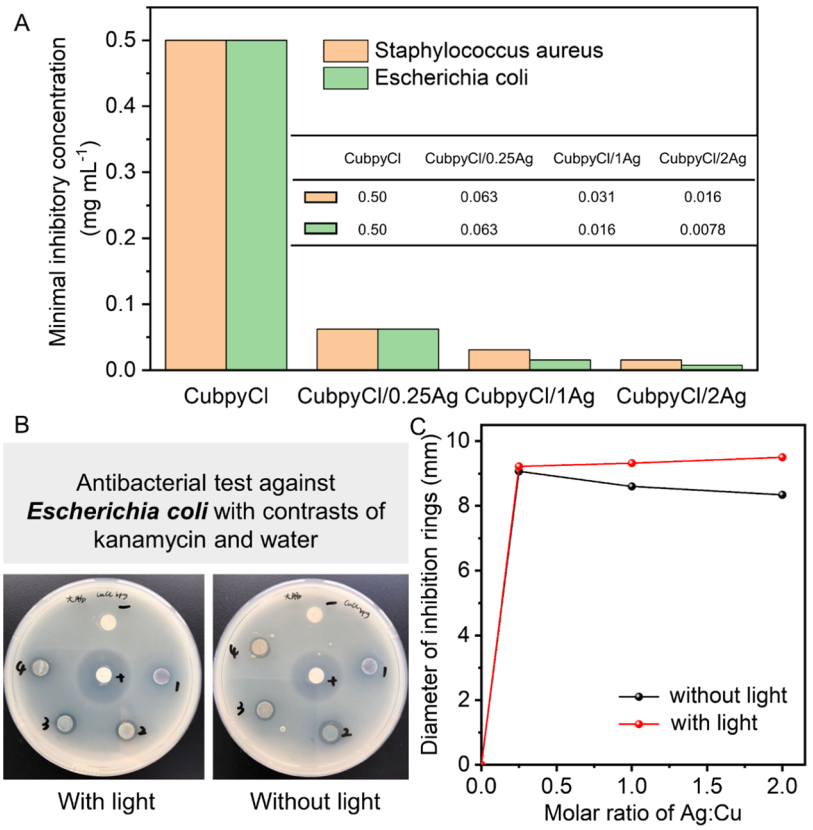


**Figure 4.** Antibacterial activity measurements. (A) MICs of CubpyCl, CubpyCl/0.25Ag, CubpyCl/1Ag, and CubpyCl/2Ag samples against S. aureus (orange) and E. coli (green) bacteria (inset table shows the specific MIC values). The enhanced sensitivity against *E. coli* is revealed by the MIC results. (B) Digital image of the antibacterial test against *E. coli* of CubpyCl, CubpyCl/0.25Ag, CubpyCl/1Ag, and CubpyCl/2Ag, in which kanamycin (+) and water (−) act as the contrasts. (C) Plots of the antibacterial ring diameter of the prepared samples with light and without light. The antibacterial activity of materials could be enhanced by light.

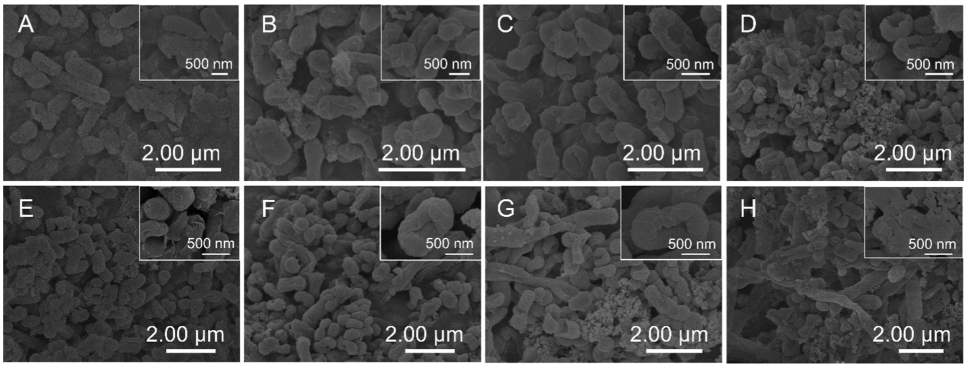


**Figure 5.** SEM images of *E. coli* incubated without light (A−D) and with light (E−H), in which CubpyCl, CubpyCl/0.25Ag, CubpyCl/1Ag, and CubpyCl/2Ag were correspondingly added. Insets show the magnified images.

bridged Cu(I) dimers act as reaction sites to in situ formed AgCl. The structure of the synthesized materials was characterized by XRD, SEM, and TEM, and the MOF phase was retained on introducing excess $Ag^+$ ions into the network. Antibacterial activity tests verified that Cu(I)MOF-AgCl/Ag exhibits an enhanced performance against *E. coli* with light irradiation.

## ■ ASSOCIATED CONTENT

### Supporting Information

The Supporting Information is available free of charge at https://pubs.acs.org/doi/10.1021/acsomega.2c07415.

Experimental chemicals and material characterization methods; energy-dispersive X-ray spectroscopy (EDS) analysis of samples; digital images of samples at various reaction times; antibacterial test against *Staphylococcus aureus*; SEM images of samples after antibacterial tests; supporting XPS and XRD of samples; SEM images of *E. coli* without antibacterial materials (PDF)

## ■ AUTHOR INFORMATION

### Corresponding Authors

**Bin Li** − *Institute of Dermatology, Shanghai Academy of Traditional Chinese Medicine, Shanghai 201203, China;*



https://doi.org/10.1021/acsomega.2c07415
*ACS Omega* 2023, 8, 2733−2739

*Department of Dermatology, Shanghai Skin Diseases Hospital, Shanghai 200443, China*; Email: 18930568129@163.com

**Peng Fei Liu** − *Key Laboratory for Ultrafine Materials of Ministry of Education, Shanghai Engineering Research Center of Hierarchical Nanomaterials, School of Materials Science and Engineering, East China University of Science and Technology, Shanghai 200237, China*; orcid.org/0000-0003-0411-0488; Email: pfliu@ecust.edu.cn

### Authors

**Fangxin Mao** − *Key Laboratory for Ultrafine Materials of Ministry of Education, Shanghai Engineering Research Center of Hierarchical Nanomaterials, School of Materials Science and Engineering, East China University of Science and Technology, Shanghai 200237, China*

**Yonghua Su** − *Department of Dermatology, Yueyang Hospital of Integrated Traditional Chinese and Western Medicine, Shanghai University of Traditional Chinese Medicine, Shanghai 200437, China; Institute of Dermatology, Shanghai Academy of Traditional Chinese Medicine, Shanghai 201203, China*

**Xiaoying Sun** − *Department of Dermatology, Yueyang Hospital of Integrated Traditional Chinese and Western Medicine, Shanghai University of Traditional Chinese Medicine, Shanghai 200437, China; Institute of Dermatology, Shanghai Academy of Traditional Chinese Medicine, Shanghai 201203, China*

Complete contact information is available at: https://pubs.acs.org/10.1021/acsomega.2c07415

### Author Contributions

F.M. and Y.S. contributed equally to this work. F.M. and Y.S. contributed to conceiving the project and conducting experiments. X.S. contributed to investigation and data analysis. B.L. and P.F.L. contributed to resources, supervision, and editing. All authors discussed the results and have given approval to the final version of the manuscript.

### Notes

The authors declare no competing financial interest.

## ■ ACKNOWLEDGMENTS

This work was financially supported by grants from the Clinical Research Plan of SHDC (No. SHDC2020CR3097B), the National Natural Science Foundation of China (52103340 and 82174383), the China Postdoctoral Science Foundation Funded Project (2020M681201), and the Shanghai Sailing Program (No. 20YF1450400).

## ■ REFERENCES

(1) Croxen, M. A.; Law, R. J.; Scholz, R.; Keeney, K. M.; Wlodarska, M.; Finlay, B. B. Recent Advances in Understanding Enteric Pathogenic *Escherichia coli*. *Clin. Microbiol. Rev.* **2013**, *26*, 822−880.

(2) Ghalehnoo, Z. R. Diseases caused by *Staphylococcus aureus*. *Int. J. Med. Health Res.* **2019**, *4*, 65−67.

(3) De Tejada, B. M. Antibiotic Use and Misuse during Pregnancy and Delivery: Benefits and Risks. *Int. J. Environ. Res. Public Health* **2014**, *11*, 7993−8009.

(4) Hajipour, M. J.; Fromm, K. M.; Akbar Ashkarran, A.; Jimenez de Aberasturi, D.; Larramendi, I. R. d.; Rojo, T.; Serpooshan, V.; Parak, W. J.; Mahmoudi, M. Antibacterial properties of nanoparticles. *Trends Biotechnol.* **2012**, *30*, 499−511.

(5) Klasen, H. J. Historical review of the use of silver in the treatment of burns. I. Early uses. *Burns* **2000**, *26*, 117−130.

(6) Zheng, K.; Setyawati, M. I.; Leong, D. T.; Xie, J. Antimicrobial silver nanomaterials. *Coord. Chem. Rev.* **2018**, *357*, 1−17.

(7) Bruna, T.; Maldonado-Bravo, F.; Jara, P.; Caro, N. Silver Nanoparticles and Their Antibacterial Applications. *Int. J. Mol. Sci.* **2021**, *22*, No. 7202.

(8) Feng, Q. L.; Wu, J.; Chen, G. Q.; Cui, F. Z.; Kim, T. N.; Kim, J. O. A mechanistic study of the antibacterial effect of silver ions on *Escherichia coli* and *Staphylococcus aureus*. *J. Biomed. Mater. Res.* **2000**, *52*, 662−668.

(9) Chernousova, S.; Epple, M. Silver as Antibacterial Agent: Ion, Nanoparticle, and Metal. *Angew. Chem., Int. Ed.* **2013**, *52*, 1636−1653.

(10) Xu, Z.; Zhang, C.; Wang, X.; Liu, D. Release Strategies of Silver Ions from Materials for Bacterial Killing. *ACS Appl. Bio Mater.* **2021**, *4*, 3985−3999.

(11) Hutter, E.; Fendler, J. H. Exploitation of Localized Surface Plasmon Resonance. *Adv. Mater.* **2004**, *16*, 1685−1706.

(12) Hou, W.; Cronin, S. B. A Review of Surface Plasmon Resonance-Enhanced Photocatalysis. *Adv. Funct. Mater.* **2013**, *23*, 1612−1619.

(13) Wang, P.; Huang, B.; Qin, X.; Zhang, X.; Dai, Y.; Wei, J.; Whangbo, M.-H. Ag@AgCl: A Highly Efficient and Stable Photocatalyst Active under Visible Light. *Angew. Chem., Int. Ed.* **2008**, *47*, 7931−7933.

(14) Li, P.-P.; Wu, H.-X.; Dong, A. Ag/AgX nanostructures serving as antibacterial agents: achievements and challenges. *Rare Met.* **2022**, *41*, 519−539.

(15) Mao, C.; Xiang, Y.; Liu, X.; Cui, Z.; Yang, X.; Yeung, K. W. K.; Pan, H.; Wang, X.; Chu, P. K.; Wu, S. Photo-Inspired Antibacterial Activity and Wound Healing Acceleration by Hydrogel Embedded with Ag/Ag@AgCl/ZnO Nanostructures. *ACS Nano* **2017**, *11*, 9010−9021.

(16) Svoboda, L.; Bednář, J.; Dvorský, R.; Rybková, Z.; Malachová, K.; Henych, J.; Matýsek, D.; Němečková, Z. Novel synthesis of Ag@AgCl/ZnO by different radiation sources including radioactive isotope 60Co: Physicochemical and antimicrobial study. *Appl. Surf. Sci.* **2020**, *529*, No. 147098.

(17) Zhang, J.; Liu, X.; Suo, X.; Li, P.; Liu, B.; Shi, H. Facile synthesis of Ag/AgCl/$TiO_2$ plasmonic photocatalyst with efficiently antibacterial activity. *Mater. Lett.* **2017**, *198*, 164−167.

(18) Zhao, M.; Hou, X.; Lv, L.; Wang, Y.; Li, C.; Meng, A. Synthesis of Ag/AgCl modified anhydrous basic bismuth nitrate from BiOCl and the antibacterial activity. *Mater. Sci. Eng., C* **2019**, *98*, 83−88.

(19) Chang, X.; Sun, S.; Dong, L.; Yin, Y. Efficient synthesis of Ag/AgCl/$W_{18}O_{49}$ nanorods and their antibacterial activities. *Mater. Lett.* **2012**, *83*, 133−135.

(20) Li, B.; Luo, Y.; Zheng, Y.; Liu, X.; Tan, L.; Wu, S. Two-dimensional antibacterial materials. *Prog. Mater. Sci.* **2022**, *130*, No. 100976.

(21) Shen, M.; Forghani, F.; Kong, X.; Liu, D.; Ye, X.; Chen, S.; Ding, T. Antibacterial applications of metal−organic frameworks and their composites. *Compr. Rev. Food Sci. Food Saf.* **2020**, *19*, 1397−1419.

(22) Nakhaei, M.; Akhbari, K.; Kalati, M.; Phuruangrat, A. Antibacterial activity of three zinc-terephthalate MOFs and its relation to their structural features. *Inorg. Chim. Acta* **2021**, *522*, No. 120353.

(23) Zhang, J.; Li, P.; Zhang, X.; Ma, X.; Wang, B. Aluminum Metal−Organic Frameworks with Photocatalytic Antibacterial Activity for Autonomous Indoor Humidity Control. *ACS Appl. Mater. Interfaces* **2020**, *12*, 46057−46064.

(24) Shams, S.; Ahmad, W.; Memon, A. H.; Shams, S.; Wei, Y.; Yuan, Q.; Liang, H. Cu/H3BTC MOF as a potential antibacterial therapeutic agent against *Staphylococcus aureus* and *Escherichia coli*. *New J. Chem.* **2020**, *44*, 17671−17678.

(25) Soltani, S.; Akhbari, K.; Phuruangrat, A. Investigation of effective factors on antibacterial activity of Pillared-Layered MOFs. *J. Mol. Struct.* **2021**, *1225*, No. 129261.

(26) Liu, Y.; Zhou, L.; Dong, Y.; Wang, R.; Pan, Y.; Zhuang, S.; Liu, D.; Liu, J. Recent developments on MOF-based platforms for antibacterial therapy. *RSC Med. Chem.* **2021**, *12*, 915−928.
(27) Han, D.; Li, Y.; Liu, X.; Li, B.; Han, Y.; Zheng, Y.; Yeung, K. W. K.; Li, C.; Cui, Z.; Liang, Y.; Li, Z.; Zhu, S.; Wang, X.; Wu, S. Rapid bacteria trapping and killing of metal-organic frameworks strengthened photo-responsive hydrogel for rapid tissue repair of bacterial infected wounds. *Chem. Eng. J.* **2020**, *396*, No. 125194.
(28) Han, D.; Li, Y.; Liu, X.; Yeung, K. W. K.; Zheng, Y.; Cui, Z.; Liang, Y.; Li, Z.; Zhu, S.; Wang, X.; Wu, S. Photothermy-strengthened photocatalytic activity of polydopamine-modified metal-organic frameworks for rapid therapy of bacteria-infected wounds. *J. Mater. Sci. Technol.* **2021**, *62*, 83−95.
(29) Wu, Y.-M.; Zhao, P.-C.; Jia, B.; Li, Z.; Yuan, S.; Li, C.-H. A silver-functionalized metal−organic framework with effective antibacterial activity. *New J. Chem.* **2022**, *46*, 5922−5926.
(30) Qi, Y.; Ye, J.; Ren, S.; Lv, J.; Zhang, S.; Che, Y.; Ning, G. In-situ synthesis of metal nanoparticles@metal−organic frameworks: Highly effective catalytic performance and synergistic antimicrobial activity. *J. Hazard. Mater.* **2020**, *387*, No. 121687.
(31) Guo, Y.-F.; Fang, W.-J.; Fu, J.-R.; Wu, Y.; Zheng, J.; Gao, G.-Q.; Chen, C.; Yan, R.-W.; Huang, S.-G.; Wang, C.-C. Facile synthesis of Ag@ZIF-8 core-shell heterostructure nanowires for improved antibacterial activities. *Appl. Surf. Sci.* **2018**, *435*, 149−155.
(32) Yang, M.; Zhang, J.; Wei, Y.; Zhang, J.; Tao, C. Recent advances in metal-organic framework-based materials for anti-*Staphylococcus aureus* infection. *Nano Res.* **2022**, *15*, 6220−6242.
(33) Zhang, X.; Peng, F.; Wang, D. MOFs and MOF-Derived Materials for Antibacterial Application. *J. Funct. Biomater.* **2022**, *13*, No. 215.
(34) Saphier, M.; Silberstein, E.; Shotland, Y.; Popov, S.; Saphier, O. Prevalence of Monovalent Copper Over Divalent in Killing *Escherichia coli* and *Staphylococcus aureus*. *Curr. Microbiol.* **2018**, *75*, 426−430.
(35) Popov, S.; Saphier, O.; Popov, M.; Shenker, M.; Entus, S.; Shotland, Y.; Saphier, M. Factors Enhancing the Antibacterial Effect of Monovalent Copper Ions. *Curr. Microbiol.* **2020**, *77*, 361−368.
(36) Peng, R.; Li, M.; Li, D. Copper(I) halides: A versatile family in coordination chemistry and crystal engineering. *Coord. Chem. Rev.* **2010**, *254*, 1−18.
(37) Shi, D.; Zheng, R.; Sun, M.-J.; Cao, X.; Sun, C.-X.; Cui, C.-J.; Liu, C.-S.; Zhao, J.; Du, M. Semiconductive Copper(I)−Organic Frameworks for Efficient Light-Driven Hydrogen Generation Without Additional Photosensitizers and Cocatalysts. *Angew. Chem., Int. Ed.* **2017**, *56*, 14637−14641.
(38) Yaghi, O. M.; Li, G. Mutually Interpenetrating Sheets and Channels in the Extended Structure of [Cu(4,4′-bpy)Cl]. *Angew. Chem., Int. Ed.* **1995**, *34*, 207−209.
(39) Graham, P. M.; Pike, R. D.; Sabat, M.; Bailey, R. D.; Pennington, W. T. Coordination Polymers of Copper(I) Halides. *Inorg. Chem.* **2000**, *39*, 5121−5132.
(40) Han, D.; Liu, X.; Wu, S. Metal organic framework-based antibacterial agents and their underlying mechanisms. *Chem. Soc. Rev.* **2022**, *51*, 7138−7169.
(41) Han, D.; Han, Y.; Li, J.; Liu, X.; Yeung, K. W. K.; Zheng, Y.; Cui, Z.; Yang, X.; Liang, Y.; Li, Z.; Zhu, S.; Yuan, X.; Feng, X.; Yang, C.; Wu, S. Enhanced photocatalytic activity and photothermal effects of cu-doped metal-organic frameworks for rapid treatment of bacteria-infected wounds. *Appl. Catal., B* **2020**, *261*, No. 118248.
(42) Cao, Y.; Zheng, R.; Ji, X.; Liu, H.; Xie, R.; Yang, W. Syntheses and Characterization of Nearly Monodispersed, Size-Tunable Silver Nanoparticles over a Wide Size Range of 7−200 nm by Tannic Acid Reduction. *Langmuir* **2014**, *30*, 3876−3882.
(43) Godfrey, I. J.; Dent, A. J.; Parkin, I. P.; Maenosono, S.; Sankar, G. Following the Formation of Silver Nanoparticles Using In Situ X-ray Absorption Spectroscopy. *ACS Omega* **2020**, *5*, 13664−13671.
(44) Liu, Q.; Zeng, C.; Ai, L.; Hao, Z.; Jiang, J. Boosting visible light photoreactivity of photoactive metal-organic framework: Designed plasmonic Z-scheme Ag/AgCl@MIL-53-Fe. *Appl. Catal., B* **2018**, *224*, 38−45.
(45) Li, M.; Li, D.; Zhou, Z.; Wang, P.; Mi, X.; Xia, Y.; Wang, H.; Zhan, S.; Li, Y.; Li, L. Plasmonic Ag as electron-transfer mediators in Bi2MoO6/Ag-AgCl for efficient photocatalytic inactivation of bacteria. *Chem. Eng. J.* **2020**, *382*, No. 122762.
(46) Zhang, C.; Gu, Y.; Teng, G.; Wang, L.; Jin, X.; Qiang, Z.; Ma, W. Fabrication of a Double-Shell Ag/AgCl/G-$ZnFe_2O_4$ Nanocube with Enhanced Light Absorption and Superior Photocatalytic Antibacterial Activity. *ACS Appl. Mater. Interfaces* **2020**, *12*, 29883−29898.
(47) Levard, C.; Mitra, S.; Yang, T.; Jew, A. D.; Badireddy, A. R.; Lowry, G. V.; Brown, G. E. Effect of Chloride on the Dissolution Rate of Silver Nanoparticles and Toxicity to *E. coli*. *Environ. Sci. Technol.* **2013**, *47*, 5738−5745.
(48) Xiao, X.; He, E.-J.; Lu, X.-R.; Wu, L.-J.; Fan, Y.-Y.; Yu, H.-Q. Evaluation of antibacterial activities of silver nanoparticles on culturability and cell viability of *Escherichia coli*. *Sci. Total Environ.* **2021**, *794*, No. 148765.


https://doi.org/10.1021/acsomega.2c07415
*ACS Omega* 2023, 8, 2733−2739